A00-36980

AIAA 2000–3868

Applications of Electrodynamic Tethers Utilizing Their Transmission-Line Characteristics

Sven G. Bilén
The Pennsylvania State University, University Park, Pennsylvania 16802
Éric Choinière and Brian E. Gilchrist
University of Michigan, Ann Arbor, Michigan 48109

36th AIAA/ASME/SAE/ASEE Joint Propulsion Conference and Exhibit
16–19 June 2000
Huntsville, Alabama

Applications of Electrodynamic Tethers Utilizing Their Transmission-Line Characteristics

Sven G. Bilén*
The Pennsylvania State University, University Park, Pennsylvania 16802
Éric Choinière† and Brian E. Gilchrist‡
University of Michigan, Ann Arbor, Michigan 48109

In this work, we use a previously developed model for the tether transmission line to examine several unique features of signals propagating on tethers as well as some of the potential applications for tether transmission lines. The model we use is implemented in SPICE, which allows the tether's transmission-line characteristics to be examined under a large array of stimuli and in a variety of system configurations. In addition, we offer a possible method for enhancing current to tethers using radio-frequency signals, which is practicable due to the transmission-line characteristics of tethers. We present results of initial experiments and particle-in-cell computer modeling of the radio-frequency enhancement.

Nomenclature

$\mathbf{B}_E$	geomagnetic flux-density vector, T
C_d	dielectric capacitance per unit length, F/m
C_{sh}	voltage-dependent-sheath capacitance per unit length, F/m
E	tether transmission-line *emf* per unit length, V/m
f	excitation frequency, Hz
I_{dc}	DC collected current per meter, A/m
I_{oml}	OML collected current per meter, A/m
j_{sh}	sheath current density, A/m^2
k	Boltzmann's constant, 1.38×10^{-23} J/K
l	tether length, m
L	transmission-line inductance per unit length, H/m
N	integer, unitless
n_e	electron plasma density, m^{-3}
n_0	undisturbed plasma density, m^{-3}
P_{rf}	RF power, W
q	charge magnitude, 1.602×10^{-19} C
r	radius, m
R	transmission-line resistance per unit length, Ω/m
r_d	radius of dielectric-coated conductor, m
R_p	plasma resistance per unit length, Ω/m
r_{sh}	ion-matrix-sheath distance, m
r_1	simulation outside radius, m
t	time, s
T_e	electron temperature, K
V_a	accelerating potential, V
v_g	group velocity, m/s
v_p	propagation (phase) velocity, m/s
V_{ac}	AC applied voltage, V
V_{dc}	DC applied voltage, V
v_{prop}	propagation velocity, m/s
$\mathbf{v}_s$	spacecraft velocity vector (relative to rotating Earth), m/s
V_{sh}	potential across voltage-dependent sheath, V
Z_0	transmission-line characteristic impedance, Ω
Z_{load}	load impedance, Ω
Γ	reflection coefficient
δ_m	magnetic skin depth, m
ε_0	free space permittivity, 8.85×10^{-12} F/m
η_p	plasma resistivity, Ω·m
λ	wavelength, m
λ_D	Debye length, m
μ_0	free-space permeability, $4\pi \times 10^{-7}$ H/m
τ_{af}	applied-voltage falltime, s
τ_{ap}	applied-voltage plateau, s
τ_{ar}	applied-voltage risetime, s
ω	angular excitation frequency, rad/s
ω_{pe}	angular electron-plasma frequency, rad/s
ω_{pi}	angular ion-plasma frequency, rad/s

Introduction

ARMED with an understanding of the propagation characteristics of electromagnetic pulses along electrodynamic tethers in the ionosphere, we can begin to examine a wide array of applications that exploit this feature. Signals, or perturbations, take a finite amount of time to propagate along a tether and tend to affect the surrounding ionospheric plasma as they travel. This interaction, in turn, affects the tether's

*Assistant Professor, Communications and Space Sciences Laboratory, AIAA Member
†EECS Graduate Student Fellow, Radiation Laboratory
‡Associate Professor, Electrical Engineering and Space Systems, AIAA Senior Member

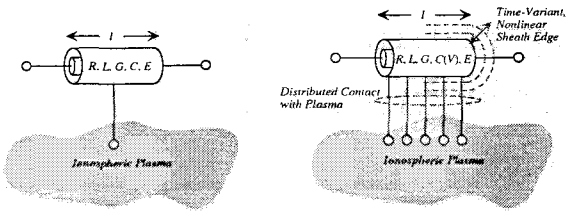

Fig. 1 Electrodynamic-tether transmission-line models: (a) static-sheath model and (b) dynamic-sheath model.

transmission-line (TL) characteristics. Under negative high-voltage excitation the sheath is dynamic and nonlinear—unlike the assumptions generally used for low excitation voltages, those being static sheath size or linearized sheath characteristics. Because the plasma effectively forms the outer conductor,[1] the geometry of the plasma–conductor system is not rigid and this dynamic and nonlinear sheath fundamentally changes the nature of EM propagation along electrodynamic tethers.

Previous tether TL models[2,3] assume, as a first-order approximation, that the plasma-sheathed tether can be modeled as a simple rigid coaxial cable (Figure 1a). While this has proven acceptable for short tethers,[4] an improved model is needed for longer deployed tether lengths, primarily to account for the higher induced voltages and the dynamic sheath. That is, in the transient case of a pulse propagating along the tether, the approximate coaxial geometry is dynamic since the surrounding plasma is affected by the pulse's passage (Figure 1b), unlike the case of typical coaxial cable which has a rigid metal sheathing.

In this paper, we will present first a TL model of the electrodynamic tether and several applications that exploit this TL nature. We then present some initial work into possible RF enhancement of current collection to bare tethers.

The Electrodynamic Tether Transmission Line

Transient plasma sheath model

Bilén and Gilchrist[5] derived a transient plasma sheath model by analytical means and verified the model by experiments and PIC simulations. The model is valid in the frequency regime between the electron and ion plasma frequencies ($\omega_{pe} \gg \omega \gg \omega_{pi}$), and for large negative applied voltages, $|V_a| \gg kT_e/q$. In this frequency regime, the E-field from the conductor is contained within the sheath region and the model describes the ion-matrix-sheath radius as a function of applied voltage, $r_{\rm sh}(V_a)$. The equation for $r_{\rm sh}(V_a)$ is

$$r_{\rm sh}(V_a) \simeq \sqrt{3}\left(\frac{V_a\varepsilon_0}{q_e n_0}\right)^{5/12} r_a^{1/6} \text{ for } r_{\rm sh} \gg r_a, \quad (1)$$

where r_a is the radius of the cylindrical conductor. This equation is an important result in that it is non-transcendental—unlike the exact expression—which allows it to be used easily as the basis of the circuit model we develop for use in the SPICE circuit-simulation code.

Electrodynamic-tether circuit model

We now employ the model of the voltage-dependent sheath as the basis of a nonlinear transmission-line model of the electrodynamic tether using the Tethered Satellite System (TSS) tether[6] as an example. The model of the tether–plasma system that we develop is, in effect, of a "non-static" coaxial transmission line, *i.e.*, a transmission line with voltage-dependent ("dynamic") parameters. In the frequency range $\omega_{pe} \gg \omega \gg \omega_{pi}$, the tether's E- and B-fields are contained locally allowing us to define an effective capacitance and inductance per unit length for the tether. In developing this model, we use the knowledge that the E-field is contained within the sheath region (as shown by Bilén[7]) to develop the effective capacitance. We then find the effective inductance by showing that the B-field is also locally contained, but in a larger region that takes into account the location of the plasma return currents.

The capacitance and inductance per unit length are based on the sheath distance, $r_{\rm sh}$, which is a function of the voltage applied across the sheath. Hence, the capacitance and inductance per unit length ultimately depend on applied voltage. Fig. 2 shows $r_{\rm sh}$ as a function of applied voltage with $r_a = 0.43$ mm (TSS-tether geometry) and $n_e = 10^{12}$ m^{-3}.

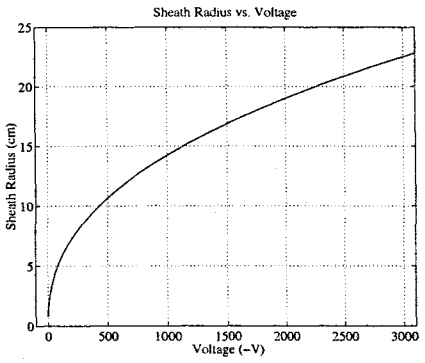

Fig. 2 Plot of ion-matrix-sheath radius, $r_{\rm sh}$, vs. applied voltage for a cylindrical tether geometry in an $n_e = 10^{12}$ m^{-3} plasma.

Coaxial capacitor approximation

Using the particle distribution shown in Fig. 3, Bilén[7] developed a model for the tether capacitance using a coaxial capacitor approximation. The derived

capacitance per unit length is given as

$$C_{\rm sh} = \frac{2\pi\varepsilon_0}{\ln\left(\frac{r_{\rm sh}}{r_a}\right)}. \qquad (2)$$

Using this simple model, we see that the cylinder–sheath–plasma system approximates a coaxial capacitor.

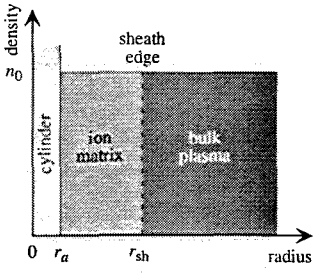

Fig. 3 Simplistic model of an RF sheath surrounding a negatively biased cylinder immersed in a plasma.

Coaxial inductance approximation

The inductance of a typical coaxial transmission line can be determined through a calculation of the stored magnetic energy of the system. In the typical coaxial line, the magnetic fields are confined to the region between the two conductors since a return current flows in the outer conductor that is equal and opposite to that of the center conductor; hence, the magnetic fields are confined. In the absence of a return conductor, as in the case of electrodynamic tethers, some other mechanism for confining the magnetic field is needed.

Although a perfectly conducting plasma will exclude a changing magnetic field just as a perfect conductor does, magnetic fields can penetrate into a plasma to a distance equal to the magnetic skin depth, $\delta_m = c/\omega_{pe}$, because of electron inertia. Equivalently, we can say that it is bulk plasma currents which flow to exclude the external field rather than surface currents at the sheath edge. A typical value of δ_m for an $n_e = 10^{12}$ m^{-3} ionospheric plasma is 5.3 m. The effect of the plasma skin depth is to cause the RF B-field generated by the current-carrying wire to diminish more quickly than it would in a vacuum.

Using the concept of magnetic skin depth described above, Bilén[7] derived the inductance of the tether to be approximately

$$L \approx L_{\rm approx} = \frac{\mu_0}{2\pi}\ln\left(\frac{\delta_m}{2r_a}\right), \qquad (3)$$

which indicates that the inductance is approximately what would be derived if all return current flowed as a surface current at a radius of $\delta_m/2$.

The inductance-per-unit-length parameter generally has been neglected in previous transmission-line models of electrodynamic tethers. For example, Arnold and Dobrowolny[2] exclude inductance and so avoid integrating the rate of change of current in their computer model. Osmolovsky *et al.*[3] include the inductance term in a generalized description of their model, but then set the inductance parameter to zero before performing calculations. In general, the absence of an inductance term in these previous models is justified because those models are not concerned with examining electromagnetic-signal propagation effects.

Tether characteristic impedance and propagation velocity

Using the parameters for capacitance and inductance per unit length, we can calculate the classical characteristic impedance of and propagation velocity along the tether transmission line. Since the capacitance is a function of voltage, then both impedance and propagation velocity are functions of voltage. Assuming $G = 0$ (insulated tether), $R \ll \omega L$, and $L =$ constant, then the characteristic impedance is given by

$$Z_0(V_a) \simeq \sqrt{L/C(V_a)}. \qquad (4)$$

Eqn. 4 is plotted in Fig. 4 for several values of plasma density; the figure clearly shows that as n_e decreases, Z_0 increases. The propagation (phase) velocity for the tether transmission line is given by

$$v_{\rm prop}(V_a) = v_p(V_a) = 1/\sqrt{LC(V_a)}. \qquad (5)$$

Eqn. 5 is plotted in Fig. 5 for several values of plasma density; the figure clearly shows that as n_e decreases, v_p increases.

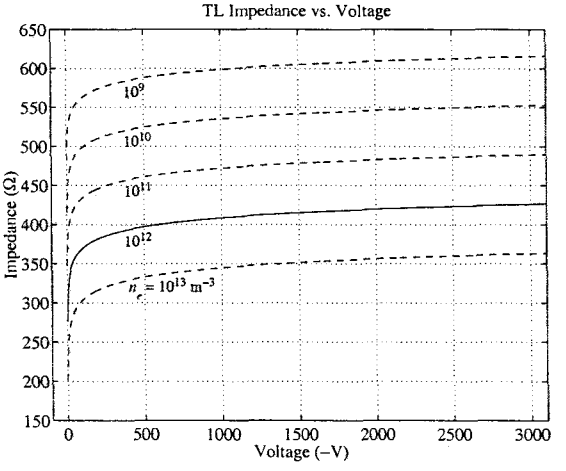

Fig. 4 Plot of tether transmission-line impedance vs. applied voltage for the cylindrical tether geometry for various plasma densities. Solid line represents an $n_e = 10^{12}$ m^{-3} plasma.

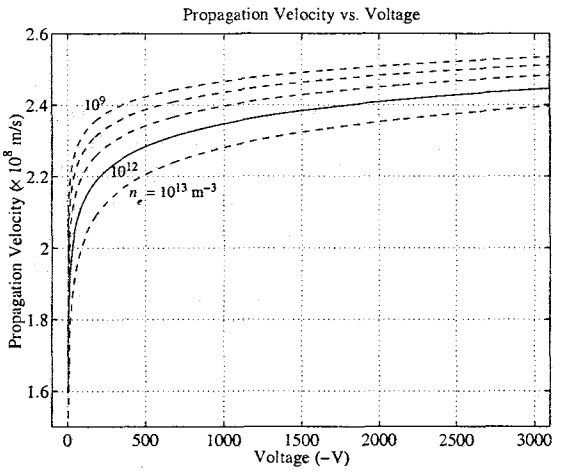

Fig. 5 Plot of tether transmission-line propagation velocity vs. applied voltage for the cylindrical tether geometry for various plasma densities. Solid line represents an $n_e = 10^{12}$ m^{-3} plasma.

Several other researchers have reported on propagation velocities along plasma-immersed conductors. James[8] experimentally determined a small-signal group speed $v_g = 0.6c \simeq 1.8\times10^8$ m/s for sheath waves along the OEDIPUS–A 958-m tether. This measurement agrees well with the model presented here, given the appropriate parameters for their system: $r_a = 0.26$ mm, $r_d = 0.66$ mm, $r_{sh} = r_a + \lambda_D \sim 1.25$ cm, and $n_e \sim 10^{11}$ m^{-3}. However, unlike the model presented here, their model was based on a voltage-independent (*i.e.*, fixed) sheath distance.

Tether incremental circuit model

The incremental circuit model of the electrodynamic tether (Fig. 6) consists of the elements R, L, E, C_d, R_p, $C_{sh}(V_{sh})$, and $j_{sh}(V_{sh})$ per unit length, Δz. The values for R, L, E, C_d, and R_p are fixed values which are either measured or calculated. The remaining two, $C_{sh}(V_{sh})$, and $j_{sh}(V_{sh})$, are varying parameters which depend on V_{sh}, the sheath voltage.

The other varying parameter we have included in the circuit model is a current-per-unit-length term that also depends on sheath voltage. Since we have confined ourselves to $\tau_{pe} \ll \tau \ll \tau_{pi}$, we are only interested in electron current because on this timescale, electrons can redistribute themselves but ions are motionless. Hence, electron current can be collected but not ion current.* The functional form for this term is that of OML current collection. Since there is no ion current collection, then for $V_{sh} < 0$, $j_{sh} = 0$.

In Fig. 6, the R_p resistance per unit length results from the plasma's specific resistivity in the return-current shell. This term is included in the return

*There is also a small ion ram current which is not included in the model.

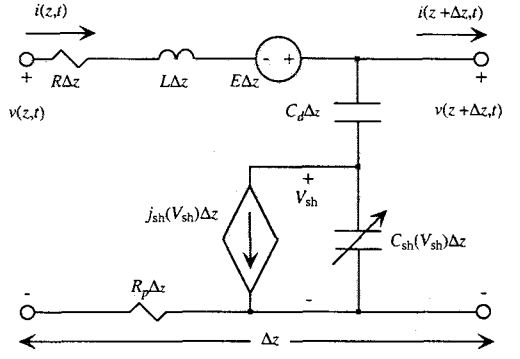

Fig. 6 Tether incremental circuit model which shows R, L, E, C_d, R_p, $C_{sh}(V_{sh})$, and $j_{sh}(V_{sh})$ per unit length, Δz.

(bottom) leg of the incremental circuit. For the TSS-tether geometry, Table 1 summarizes the parameters for the incremental circuit model with the assumption, when required, of an $n_e = 10^{12}$ m^{-3}, $T_e = 1160$ K ionospheric plasma.

Table 1 TSS transmission-line circuit parameters per unit length. Typical values are given for an $n_e = 10^{12}$ m^{-3}, $T_e = 1160$ K ($\theta_e = 0.1$ eV) ionospheric plasma.

Parameter and Equation	Typical Value
R —	0.103 Ω/m
$L \simeq \frac{\mu_0}{2\pi}\ln\left(\frac{\delta_m}{2r_a}\right)$	1750 nH/m
$E = -\lvert\mathbf{v}_s \times \mathbf{B}_E\rvert$	−0.2 V/m
$C_d = \frac{2\pi\varepsilon_d}{\ln\left(\frac{r_d}{r_a}\right)}$	128 pF/m
$R_p \sim \frac{\eta_p}{\pi\delta_m^2}$	0.5 mΩ/m
$C_{sh}(V_{sh}<0) \simeq \frac{2\pi\varepsilon_0}{\ln\left[\frac{\sqrt{3}}{r_d}\left(\frac{V_{sh}\varepsilon_0}{q_e n_0}\right)^{5/12} r_a^{1/6}\right]}$	$\frac{134}{\ln(6.3\lvert V_{sh}\rvert)}$ pF/m
$j_{sh}(V_{sh}>0) = 2\sqrt{2}r_d n_{e0} q_e v_{te}\sqrt{\frac{qV_{sh}}{kT_e}}$	$-240\sqrt{V_{sh}}$ μA/m

SPICE implementation of incremental circuit model

Transient simulations of the circuit model were performed using HSPICE (version H96) software developed by Meta-Software, Inc., which is similar to the standard Berkeley SPICE. The electrodynamic-tether circuit model was implemented as an HSPICE deck with which transient analyses could be performed.

The entire tether circuit is assembled as a ladder network of N incremental sections of length chosen such that $\Delta z \ll \lambda$. A choice of 4-m increments for Δz yields a minimum of 40 increments per wavelength. A circuit consisting of $N = 5000$ increments was used, which equates to an 20-km-long tether. This length was chosen for two reasons: 1) 20-km is the length of practical tether systems such as TSS and 2) this length allows the applied pulses and sinusoidal waveforms to

be adequately resolved at different sections along the transmission line.

For tether systems, there are several methods for producing tether voltage modulations, *i.e.*, forced oscillations, which include 1) periodically producing current increases, decreases, or breaks; 2) varying the source and/or load impedances; and 3) changing parameters and control voltages of the contactors and emitters. For these circuit simulations, we utilize a voltage source controlled by pulse and sinusoidal functions.

SPICE Simulation Results

A sample simulation that employed pulse excitation of the transmission line is given here. The applied pulse had the following properties: voltage magnitude across sheath, $V_{\rm sh} \sim -570$ V; $\tau_{ar} = \tau_{ap} = \tau_{af} = 1$ μs. Fig. 7 shows the simulation results for a lossless line where R and $R_p \simeq 0$. The figure plots the sheath voltage, $V_{\rm sh}$, on linear and log scales and sheath capacitance, $C_{\rm sh}$, as a function of time for five positions along the transmission line: section $N = 1$ (initial), $N = 1000$, $N = 2000$, $N = 3000$, and $N = 4000$. Every 1000 sections represents 4 km. Note that the time axis increases to the right, which means that signals located more to the right occur *later* in time.

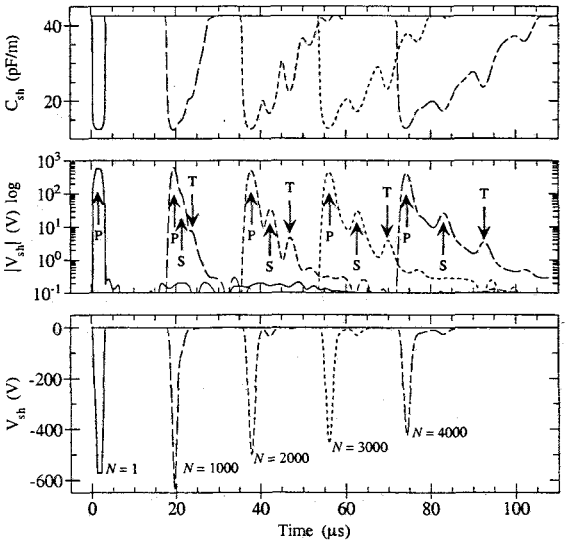

Fig. 7 Transient SPICE simulation of an excited high-voltage pulse on the lossless tether transmission line. Plotted are the voltage across the sheath, $V_{\rm sh}$, on linear and log scales and the sheath capacitance, $C_{\rm sh}$, as a function of time. The five curves represent values at the indicated section number of a 5000-section (20-km) tether transmission line.

In Fig. 7, it is interesting to note that the width of the primary disturbance (marked "P") remains approximately the same as it travels the length of the transmission line, although it becomes reduced in magnitude. In addition to the primary pulse, a lower-voltage tail at the trailing edge of the pulse (marked "S") begins to form. This secondary pulse can already be seen at section $N = 1000$, but becomes more pronounced at later sections. A tertiary pulse (marked "T") also forms and propagates at an even slower velocity since its voltage is lower still. The formation of additional pulses is not completely unexpected behavior, since we know that higher voltages travel faster along the line due to their increased propagation velocity as compared to lower voltages.

Sinusoidal Excitation

The second type of simulation excited the transmission line with an RF sinusoid that had the following properties: voltage magnitude across sheath, $V_{\rm sh} \sim -1200$ V; $f = 100$ kHz.[†] Figure 8 plots the results of this RF-sinusoidal excitation simulation at various points along the lossless line (R and $R_p \simeq 0$). The figure plots the sheath voltage, $V_{\rm sh}$, and sheath capacitance, $C_{\rm sh}$, as a function of time for three positions along the transmission line: sections $N = 1$ (initial), $N = 2000$, and $N = 4000$.

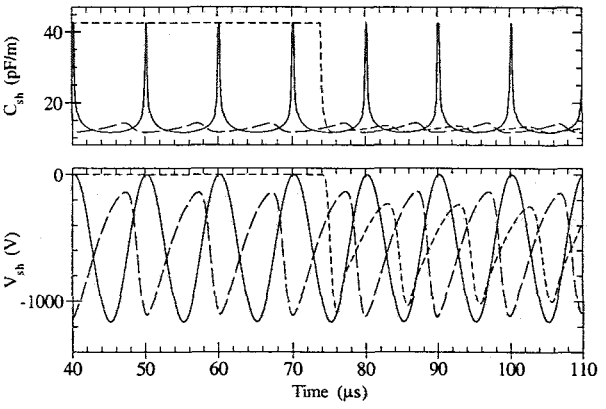

Fig. 8 Transient SPICE simulation of a high-voltage 100-kHz sinusoid excited on the lossless tether transmission line. Plotted are the voltage across the sheath, $V_{\rm sh}$, and the sheath capacitance, $C_{\rm sh}$, as a function of time. The three curves represent values at sections $N = 1$ (initial, solid line), $N = 2000$ (long-dashed), and $N = 4000$ (short-dashed) sections of a 5000-section (20-km) tether transmission line.

The RF-sinusoidal excitation simulation shows the very important result that the sinusoidal waveform steepens as it propagates along the transmission line—an effect noticed on many other nonlinear transmission lines. Because of this steepening effect, significant harmonic distortion will be added to any signal propa-

[†]Strictly speaking, this frequency does not satisfy the criterion $f \gg f_{pi}$. However, there was some attenuation that was much more pronounced at the higher frequencies, so a lower frequency was used here.

gating along the transmission line. An analysis of this added harmonic distortion was made by taking FFTs of the waveform at various points along the transmission line and plotting the energy in the fundamental and the first four harmonics. The results of this analysis are plotted in Fig. 9. What is seen in this figure is that the harmonic amplitudes quickly build up within the first 4 km and then much more slowly thereafter; the energy in the harmonics comes from the energy in the fundamental. This is important information for several reasons: 1) the quick buildup in the harmonics means that for all practical tether lengths, the propagated signal is likely to be distorted; 2) for long tether lengths the distortion builds up much more slowly after the initial buildup.

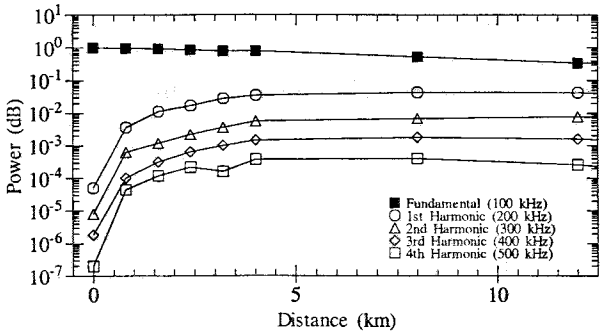

Fig. 9 FFT-derived powers in the fundamental and first four harmonics of a propagating sinusoid as a function of distance along the tether transmission line.

Tether circuit-model applications

Some potential applications for and the utility of the circuit model developed here include 1) prediction of time-domain reflectometry responses along the tether transmission line from which it may be possible to reconstruct impedance profiles; 2) prediction of pulse and waveform propagation morphology; and 3) prediction of overall tether system responses to various stimuli when implemented together with endpoint models. We dicuss the first two below and refer the reader to Bilén[7] for the third.

Time-domain reflectometry

Time-domain reflectometry (TDR), also sometimes known as pulse reflectometry, is a technique which consists of sending an impulse down a transmission line and recording the reflected energy—the "echo"—as a function of time. The reflected TDR waveform measurement provides insight into the physical structure of the device under test (DUT). The characteristics of the DUT(s) can be determined from knowledge of both the incident and reflected signals. The TDR technique has the advantage of being able to accurately model nonlinear devices.[‡]

The shortest pulse length that can be launched onto this transmission-line model is on the order of $\tau_a = 1$-3 μs for an $n_e = 10^{12}$ m^{-3} plasma. This pulse length, in turn, places a lower limit on the spatial resolution of any TDR measurements. To get a idea for what kind of resolution is possible with a TDR measurement, a 3-μs, -500–V pulse traveling $\sim 2.3 \times 10^8$ m/s yields a minimum spatial resolution $\gtrsim 700$ m.

Several simulations were run to ascertain if TDR can be used as a novel application of electrodynamic tethers. Fig. 10 shows one such simulation wherein a pulse was launched along a lossless tether transmission line that had a step discontinuity in plasma density (from $n_e = 10^{12} \rightarrow 10^{10}$ m^{-3}) at section $N = 3000$; the value of Z_{load} was left at the $Z_0(0)$ value of the first portion of the line. Although somewhat artificial, such a situation could occur if the upper half of the tethered system were to fly into a deep density depression with sharply defined features. The simulation results show very clearly two return pulses, the first is due to the change in plasma density at $N = 3000$ and the second is due to the mismatch at the load. Do these reflections make sense in the classic sense of TDR? To answer this, we remember that the reflection coefficient, Γ, at an impedance discontinuity on a transmission line is given by the equation

$$\Gamma = \frac{Z_{\text{load}} - Z_0}{Z_{\text{load}} + Z_0}, \tag{6}$$

where Z_{load} is either a load impedance or a new transmission line impedance. (Note: this equation does not take into account the voltage dependencies of the characteristic impedance.) As plasma density decreases, Fig. 4 shows that Z_0 increases. Hence, at the step change in plasma density we would expect a positive Γ, and indeed the return pulse from this discontinuity is the same polarity. Conversely, at the load we would expect a negative Γ, and indeed the return pulse from the load is positive. This simple demonstration shows that TDR applications along tethers may hold promise for future systems.

Predictions of pulse and signal morphology

This circuit model promises to have utility for examining the propagation of undesirable high-voltage signals along the lengths of structures in ionospheric plasma. In addition, with signals for which propagation is desired, this model can help to understand and predict the manner in which the signal will mutate from its original shape. Such predictive simulations should help to ascertain, for example, how much harmonic distortion is added to a high-voltage RF signal

[‡]Nowadays, the TDR technique is often accomplished by applying a Fourier transform to frequency-domain data. While the transform technique has found much utility, especially for microwave-circuit measurements, the "old" method of applying an actual pulse continues to find areas of use.

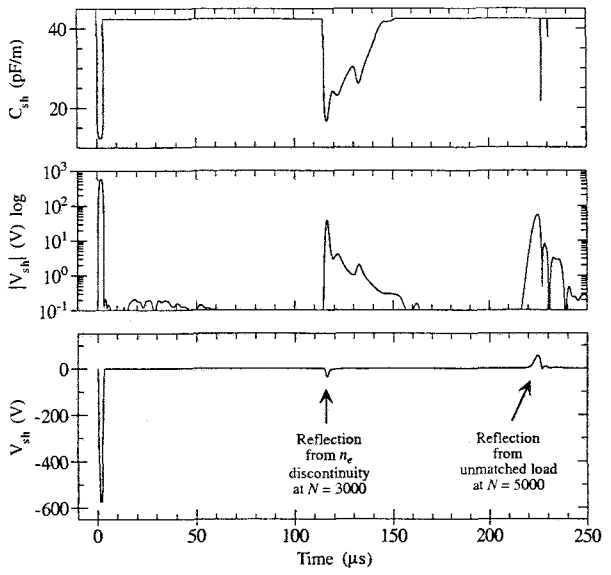

Fig. 10 Time-domain-reflectometry simulation with a pulse along a lossless tether transmission line that had a step discontinuity in plasma density and a unmatched load impedance.

on the tether. The utility of this model for determination of harmonic-distortion estimation was shown above.

Radio-Frequency Enhancement of Tether Electron Collection

One of the main limiting factors for increased thrust in bare electrodynamic tether systems is the current collection limit, which is determined by the given plasma characteristics and tether geometry. The use of radio-frequency signals is proposed here as a means of increasing the electron collection on a bare tether.

Breaking through the OML current limit

Under steady-state DC conditions, the amount of current collected by a positively biased long circular cylinder such as a tether immersed in a low-density plasma is limited by the orbital-motion-limited (OML) current law, which is based on conservation of angular momentum.[9] The proposed current enhancement technique seeks to enhance current collection beyond this apparent limit through the injection of a radio-frequency signal superposed on the bias potential and propagated along the transmission line formed by the tether sheath structure.§

Analogous to what has been observed with spherical probes,[10] a resonance condition on the tether sheath structure was experimentally observed on a cylindrical tether simulator, which occurred at a frequency slightly less than the electron plasma frequency. Experimental tests were first performed that consisted of applying a 15-V_{rms} signal onto a bare 10-cm-long tungsten tether simulator that had a 140-V_{dc} bias applied to it. The simulated tether was immersed in a Xe^+–electron high-density ($\sim 10^{14}$ m^{-3}) plasma. The tether was sized such that $\lambda_D \sim 1$–$3\ r_a$. Results indicated that a large increase in the collected current occurred over a narrow frequency band centered at a frequency slightly less than the electron plasma frequency.

Particle-in-cell model and issues

The particle-in-cell (PIC) technique was used in order to model the tether-plasma interactions and characterize the enhancement phenomenon that previously was observed experimentally. A 1-dimensional cylindrical implementation of this technique[11] was adapted and used to this end. The analysis of the simplified problem is based on assumptions of a collisionless plasma, a negligible plasma drift velocity, quasi-static electromagnetic fields, and no external magnetic field. Another important assumption concerns the ion density distribution, which is assumed to be uniform everywhere around the tether; this is the well-known *matrix sheath* approximation.[12]

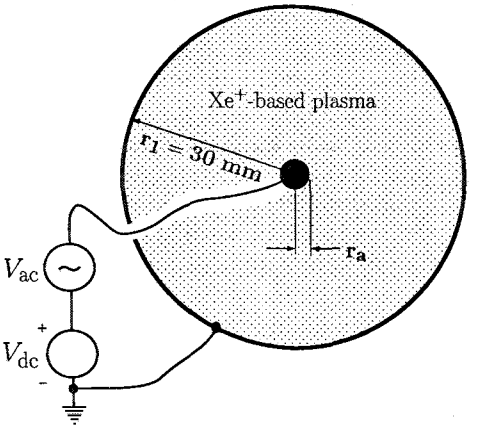

Fig. 11 Basic geometry of the simplified model of the electrodynamic tether problem.

Fig. 11 depicts the geometry of our simplified model. An outer perfect electric conductor at $r = r_1$ is used as the boundary condition representing the plasma potential reference, arbitrarily set to zero here. The potential difference between the center and outer conductor is set to a sinusoidal potential variation of amplitude V_{ac} on top of a bias potential V_{dc}. It should be noted that the `xpdc1`[11] code has been modified such that the number of electrons present in the simulation domain remains constant during the simulation. That is, for every electron collected either on the tether or on the outer conductor, another electron is emitted

§The work of this section employs a positive DC bias on a bare tether. As a point of contrast, the transmission-line model of the previous section was developed for negative, transient pulses on an insulated tether. Hence, the tether sheath structures will be different.

from the outer conductor with its three velocity components chosen according to a Maxwellian distribution at the bulk plasma electron temperature.

Because of memory and computing power limitations, individual electrons cannot all be included in the simulations. Instead, a reduced number of large particles with larger charge and mass are simulated. The ratios used for the number of real electrons to the number of simulated particles were in the range of 10^7 to 10^8. In order to compensate for noise in the simulation diagnostics caused by the artificial granularity of the simulation, results were averaged over many RF cycles after an initial delay. Many diagnostics were computed using this averaging technique, among which the average collected DC current (I_{dc}), average sheath width, the fundamental and harmonics of the time-varying current response, the average RF power dissipated in the sheath (P_{rf}), the input impedance, and the steady-state time periodic electric field distribution.

Basic physics of the enhancement phenomenon

From the PIC simulations, an evaluation of the steady-state time periodic electric field distribution (a function of r and t) was obtained from averages over several RF cycles. This steady-state, time periodic field is a solution that accounts for all electron plasma dynamics around the tether. Running a test particle (an electron) through this field-solution allows one to predict its trajectory as a function of initial position, velocity, and time of release with respect to the phase of the applied RF signal on the tether.

Fig. 12 shows the trajectories of two test electrons with identical initial conditions through both a DC potential distribution (no RF excitation on the tether) and an RF-enhanced potential distribution. For the case presented here, the initial angular momentum of the electron is too large compared to its radial velocity for it to be collected by the tether with the DC excitation alone. The RF enhancement, however, results in the scattering of the electron from the OML trajectory. In the illustrated case, the electron running through the RF-enhanced field is collected. The DC bias was 120 V in both cases and the RF signal added in the second case had an amplitude of 10 V and a frequency of 75 MHz, that is, lower than the electron plasma frequency of 152 MHz corresponding to an electron plasma density of 2.9×10^{14} m^{-3}.

Although Fig. 12 illustrates a case where the electron running through the RF-enhanced field is collected, this is so only for a certain range of "release phases" measured with respect to the phase of the RF signal source. However, part of the electron population incoming at an incidence angle of 16.6 degrees with the same velocity will be collected, whereas none are in the DC case. On the other hand, an adverse effect is that some of the electrons that would normally be collected under DC conditions (at lower incidence angles, for example) might be scattered off the collection trajectory and be repelled. Although only the collective behavior formed by the combination of all scattered trajectories will determine whether electron collection is increased or decreased from the DC situation, this simple analysis illustrates how RF excitation might lead to current enhancement.

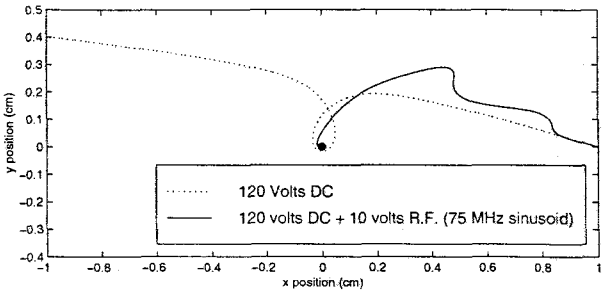

Fig. 12 Trajectories of two test electrons through the steady-state, time-periodic potential distributions around a tether computed using a particle-in-cell code. Both test particles are incident at the thermal velocity (corresponding to $T_e = 0.8$ eV) and an incident angle of 16.6 degrees off the horizontal from the right-hand side. The first electron escapes (is not collected) while the second one, being scattered off the OML trajectory by RF oscillations, is collected.

Table 2 Parameters of interest for both experiments.

Parameter	Experiment 1 (21 Dec. 1999)	Experiment 2 (19 Feb. 2000)
n_e	9.4×10^{14} m^{-3}	2.9×10^{14} m^{-3}
r_a	0.115 mm	0.14 mm
l	10 cm	29.4 cm
V_{dc}	140 V	120 V
V_{ac}	21.2 V	10 V
T_e	$\sim$ 1–2 eV	$\sim$ 1–2 eV
f_{pe}	275 MHz	152 MHz
I_{oml}	24.2 mA	24.5 mA

Simulation and experimental results

Two different configurations were investigated both experimentally and using the 1-d cylindrical PIC model. The experimental measurements were performed at the Plasmadynamics and Electric Propulsion Laboratory (PEPL) at University of Michigan, in the Large Vacuum Test Facility (LVTF). In both cases, a cylindrical tether was immersed in a Xenon-based plasma generated by the Hall-effect P5 thruster,[13] developed by the PEPL research group. Specific parameters for both experiments are listed in Table 2.

It should be noted that the values used here for n_e were obtained by calibrating the model in order to fit the simulated and experimental resonances. These approximations agree fairly well with those experimen-

tally determined via Langmuir probe and resonance probe measurements. (These experiments were performed along with two sets of experiments that examined the DC current collection to bare cylinders ins a high speed plasma flow. More information on the experimental setup and conditions may be found in Gilchrist *et al.*[14]) Also, all simulation results presented here were computed using the PIC technique with an nc2p (a parameter representing the number of actual particles to simulated particles) of 10^7 and a time step $dt = 2.5 \times 10^{-11}$ s.

First configuration

A 10-cm-long tether was tested first. Fig. 13 presents a comparison of simulation and experimental results for the DC collected current. Both responses show a resonance near 198 MHz, where an enhancement of electron collection is observed.

In the experiment, an enhancement of approximately 750% was observed for the DC current. However, the levels of enhancement of simulated and experimental results cannot be compared, because the actual voltage on the tether could not be controlled with the experimental configuration that was used. The simulation results, which were realized under conditions of constant input voltage amplitude, show an enhancement of the order of 70% at the 198 MHz resonant frequency. Another major distinction between the simulations and measurements is the bandwidth of the enhancement, which was much smaller in the experiment than in the simulations.

As expected, the enhancement effect of DC current is associated with an increase of the time-average sheath width, which is shown in Fig. 14; this increase near the resonance frequency of 198 MHz can be seen even though convergence of the curves has not been obtained due to computing time limitations. The enhancement of the average sheath signifies that the "radius of influence" of the tether on electrons is increased, allowing it to attract a larger number of electrons.

The resonance condition on the DC current collection comes about because the input reactance of the plasma-immersed tether crosses zero at $f = 198$ MHz, which results in a peak of the injected RF power (see Fig. 15) since we have an ideal voltage source. In our collisionless model, all RF power is transformed into radially-directed kinetic energy of the local electron plasma, which seems to be the fundamental mechanism leading to the increase of sheath size and the enhancement of electron collection.

Because the RF power level is varying over frequency, simply comparing levels of DC current enhancement for a fixed RF voltage does not yield a useful figure-of-merit. As can be seen in Fig. 16, the DC current enhancement is proportional to the input RF power. Thus, a useful figure-of-merit would be

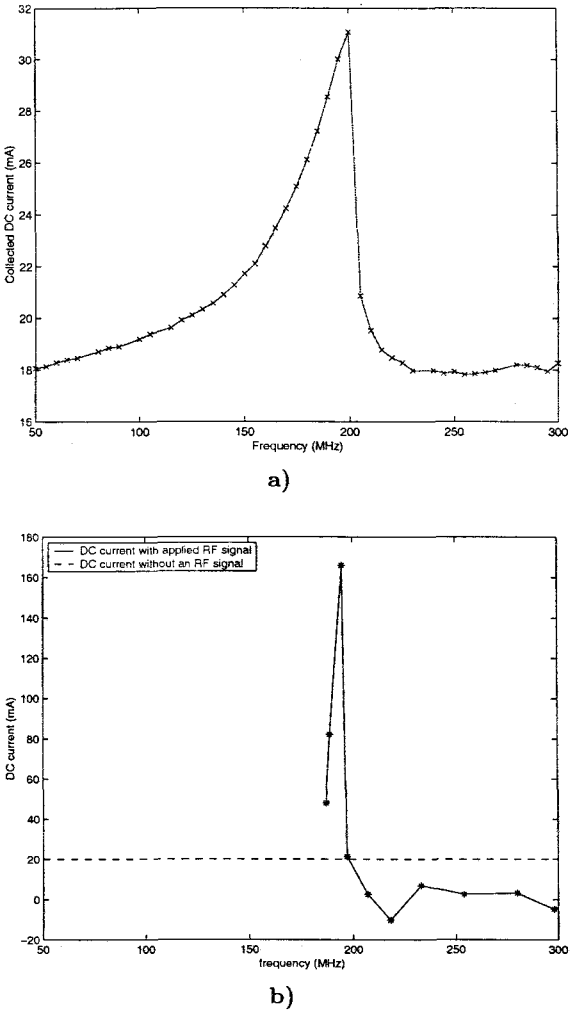

Fig. 13 DC collected current (configuration 1): (a) simulated, (b) measured.

the relative current enhancement per unit watt of RF power per meter; that is, the relative variation of DC current when 1 W of RF power is injected for every meter of tether.

Fig. 17 depicts this figure-of-merit for the simulation results. Results are approximate, because the reference level for the DC current without RF excitation have been taken as the $f = 50$ MHz data, for which a small but non-zero RF power was injected. However, it can clearly be seen from the graph that the optimum current enhancement does not occur at the resonant frequency $f = 198$ MHz, which actually presents a local minimum. The "lowest cost" of current enhancement occurs near $f = 90$ MHz, much lower than the resonant frequency; a current enhancement on the order of 8% is obtained for every watt of RF power injected per meter of tether length. This optimum frequency corresponds to a region of high non-linear behavior; note that this peak occurs in spite of the low level of injected RF power at this frequency (Fig. 15).

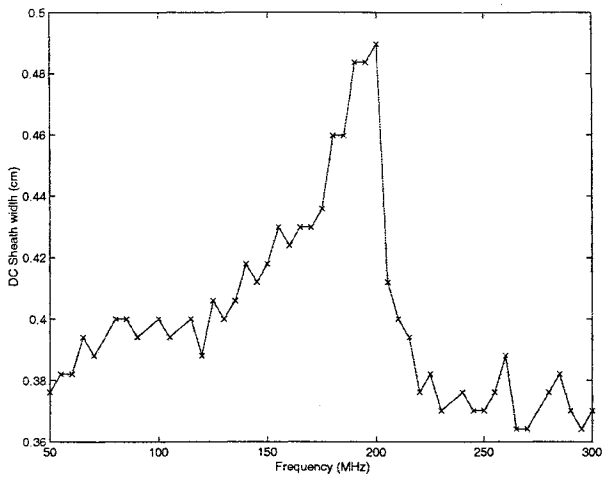

Fig. 14 Sheath width (configuration 1).

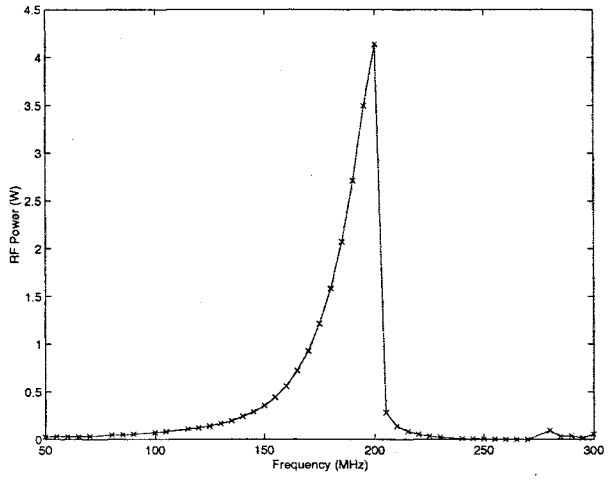

Fig. 15 Injected RF power (configuration 1).

The sharp drop after $f = 220$ MHz in the relative current enhancement shown on Fig. 17 might explain the dip in the measurements (Fig. 13b) occurring near the same frequency, if one assumes that the injected RF power level was approximately constant during the experiment. This drop is expected since reactance is nearly singular around 250 MHz.

Second configuration

The second experiment involved a 29.4-cm-long tether. Comparative results for the collected current are shown in Fig. 18. Part (a) shows the simulation result and part (b) shows measurements with uncontrolled RF voltage amplitude. The general level of the curves are somewhat different ($\sim$ 15 mA for the simulation and $\sim$ 30 mA for the measurements). Actually, the experimental result without RF excitation ($I_{dc} = 30$ mA) is about 24% higher than the OML prediction for the particular geometry considered here. This difference might be explained by the ion drift, which was neglected for the simulations and is known to have an enhancing effect on electron collection.[15]

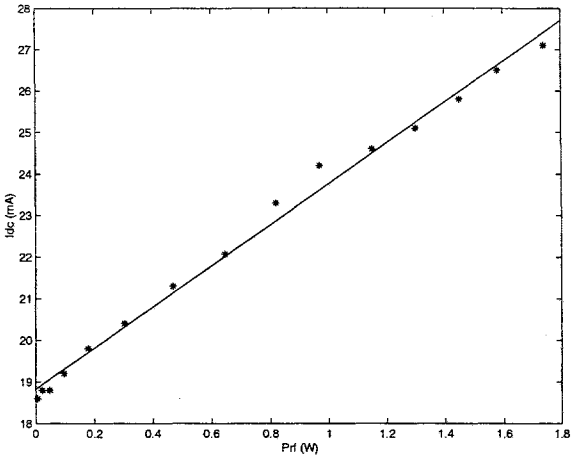

Fig. 16 DC collected current as a function of input RF power for a typical PIC simulation of a tether.

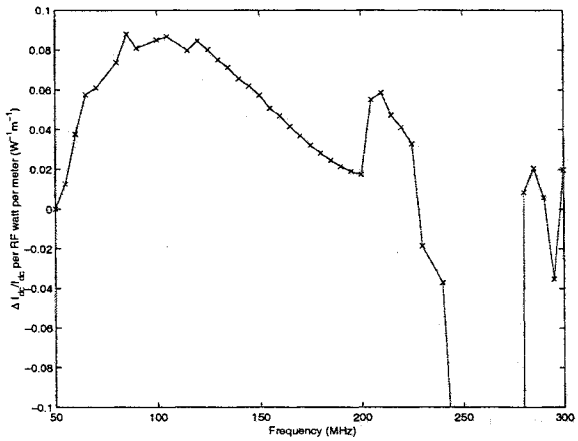

Fig. 17 Relative variation of DC current per meter of tether per watt of RF power injected (configuration 1).

The low simulation results compared with OML theory are attributed to the matrix sheath approximation for the ion density profile; further simulations should account for a more realistic ion density profile.

Nevertheless, behavior of the curves around these reference values can still be compared. Both results exhibit a resonance near $f = 117$ MHz, which results in a current enhancement of about 9 mA for the simulation case and about 1 mA for the experiment case. The sheath width (Fig. 19) is seen to grow at resonance, which is how the tether ends up gathering more electrons. The vanishing of the reactance near $f = 117$ MHz is seen to result in maximum RF power (Fig. 20), as was observed for configuration 1.

Two features of interest that do not appear in the simulation results show up in the experiment results: a maximum current enhancement near 65 MHz and an anti-resonance near 130 MHz. Those effects would presumably be explained using the figure-of-merit that was developed earlier. Fig. 21 presents the simulated

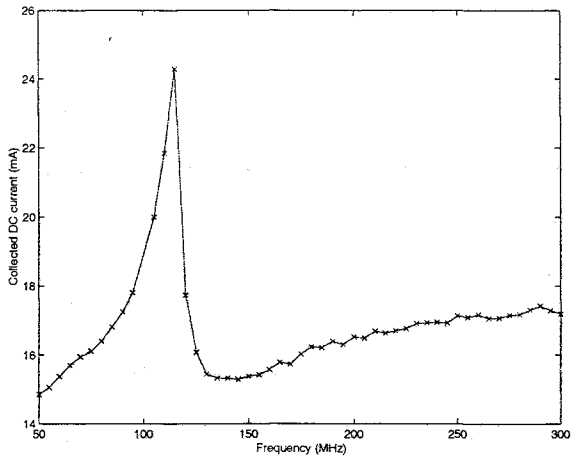

a)

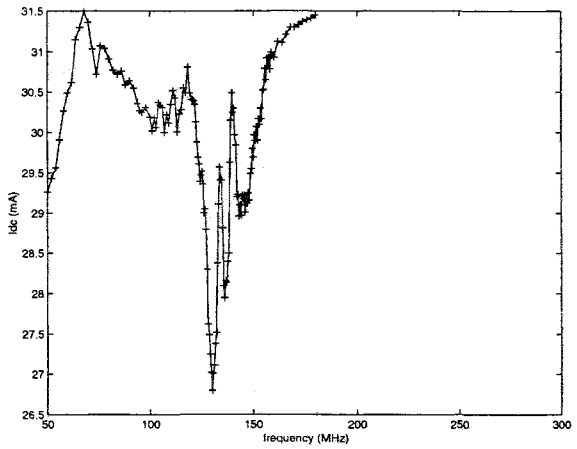

b)

Fig. 18 DC collected current (configuration 2): (a) simulation with an RF amplitude of 10 V; (b) measurements with varying RF amplitudes.

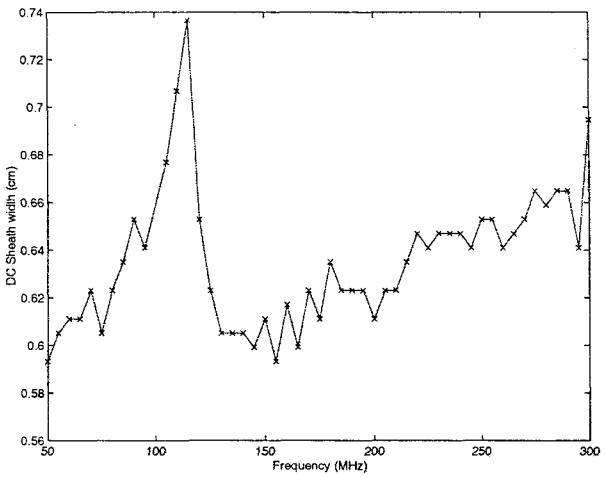

Fig. 19 Sheath width (configuration 2).

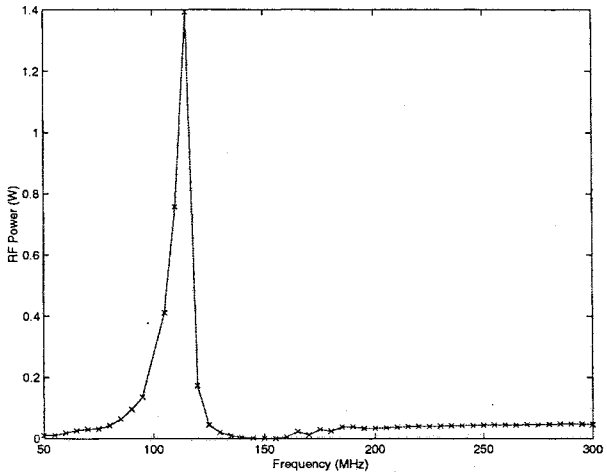

Fig. 20 Injected RF power (configuration 2).

relative variation of the DC collected current per RF watt per meter.

The relatively large levels of enhancement predicted by the simulation (around 78% at low frequencies, $\sim$ 75 MHz) were not obtained during the experiment, which showed enhancement levels of about 8%. Although the two enhancement levels differ, some important features which appear in the experimental results also show up in the simulation curves, *i.e.*, a large peak in the current enhancement around 75 MHz and another smaller peak near resonance at 117 MHz. Even though the computed figure-of-merit is very high around 150 MHz, virtually no power (see Fig. 20) is being radiated due to the singular reactance at the plasma electron frequency (f_{pe} = 152 MHz), which explains the large dip observed experimentally in the same frequency range. There also is an increased enhancement as the frequency is increased even further. For practical purposes however, the lower frequencies present more interest because of the availability, low cost, and lower losses associated with lower frequency hardware.

Summary

This research investigated and characterized the general propagation behavior of electromagnetic pulses along electrodynamic tethers in the ionosphere, and in particular, the TSS tether. This investigation first developed a voltage-dependent sheath model valid in the frequency regime between the electron and ion plasma frequencies and for negative high voltages. The sheath model was developed analytically and verified via plasma-chamber experiments and particle-in-cell computer simulations.

Using this voltage-dependent sheath model, a circuit model was developed for electrodynamic-tether transmission lines that incorporates the high-voltage sheath dynamics. The transmission-line circuit model was implemented with the circuit-simulation program SPICE, which allows complete tether systems to be

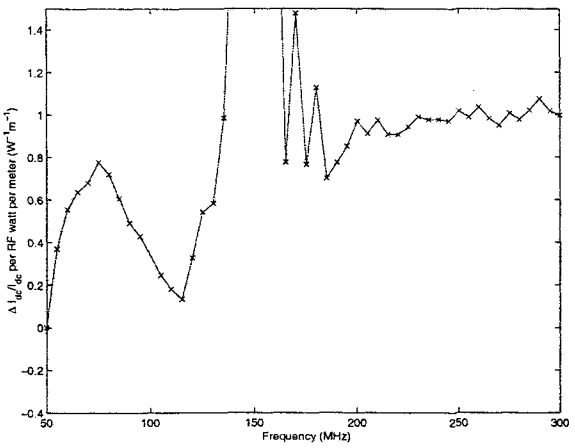

Fig. 21 Relative variation of DC current per meter of tether per watt of RF power injected (configuration 2).

modeled by including circuit models of the endpoints (which "launch", or produce, the perturbations on the tether) with the tether model itself.

Initial assessment for the injection of radio-frequency power on bare tethers as a means of enhancing electron collection in the OML regime was realized using a PIC 1-d cylindrical model and experimental measurements. Large current enhancements were obtained via simulation at resonance frequencies of the input reactance (*i.e.*, where $X_{\text{in}} = 0$), but at the expense of high RF power. On one occasion, a current enhancement of 750% was observed experimentally for an unknown input RF power level.

Since current enhancement is a linear function of the RF input power level, current enhancement is best measured with the relative current variation per unit of RF power along a 1-m section of a tether. Using that figure-of-merit, current enhancements up to 78% per meter of tether per RF watt were obtained by simulation at frequencies lower than the resonant frequency (near 75 MHz). The main features of that figure-of-merit were confirmed by experimental measurements, although at a much lower level. This difference is attributed to losses that were not accounted for in the measurement set-up.

Further investigations should include a thorough analysis of the convergence problem in the PIC model, a comparison of the present simulation results based on the ion-matrix approximation with results obtained when using a Boltzmann distribution for ions based on time-averaged potential and accounting for the ponderomotive force. Also, an experiment with controlled power and loss levels should be realized, enabling the direct measurement of the current enhancement figure-of-merit which was presented here.

Acknowledgments

The authors would like to thank Prof. A. Gallimore for use of the PEPL chamber and the PEPL research group for help in performing these experiments. We also wish to thank Dr. V. Liepa for the loan of several RF sources to perform the experiments.

References

[1]James, H. G., Balmain, K. G., Bantin, C. C., and Hulbert, G. W., "Sheath Waves Observed on OEDIPUS A," *Radio Science*, Vol. 30, No. 1, 1995, pp. 57–73.

[2]Arnold, D. A., and Dobrowolny, M., "Transmission Line Model of the Interaction of a Long Metal Wire with the Ionosphere," *Radio Science*, Vol. 15, No. 6, 1980, pp. 1149–1161.

[3]Osmolovsky, I. K., Oyama, K.-I., Sasaki, S., and Savich, N. A., "Electric Oscillations in the Electrodynamic Tethered Space Systems," *ISAS Research Note 519*, Institute of Space and Astronautical Science, Sagamihara, Japan, October 1992.

[4]Bilén, S. G., Gilchrist, B. E., Bonifazi, C., and Melchioni, E., "Transient Response of an Electrodynamic Tether System in the Ionosphere: TSS-1 First Results," *Radio Science*, Vol. 30, No. 5, 1995, pp. 1519–1535.

[5]Bilén, S. G., and Gilchrist, B. E., "Transient Plasma Sheath Model for Thin Conductors Excited by Negative High Voltages with Application to Electrodynamic Tethers," in press, *IEEE Trans. Plasma Sci.*, 2000.

[6]Bonifazi, C., Svelto, F., and Sabbagh, J., "TSS Core Equipment: I—Electrodynamic Package and Rationale for System Electrodynamic Analysis," *Il Nuovo Cimento*, Vol. 17C, No. 1, 1994, pp. 13–47.

[7]Bilén, S. G., "Pulse Propagation Along Conductors in Low-Density, Cold Plasmas as Applied to Electrodynamic Tethers in the Ionosphere," Ph.D. thesis, 332 pp., Univ. of Michigan, 1998.

[8]James, H. G., "Tether Phenomena Observed in the OEDIPUS-A Experiment," in *The Behavior of Space Systems in the Space Environment*, R. N. DeWitt *et al.*, Editors, *NATO ASI Series, Series E, Applied Sciences, No. 245*, Kluwer Academic, Norwell, MA, 1993, pp. 581–603.

[9]Sanmartín, J. R., and Estes, R. D., "The Orbital-Motion-Limited Regime of Cylindrical Langmuir Probes," *Physics of Plasmas*, Vol. 6, No. 1, 1999, pp. 395–405.

[10]Lepechinsky, D., "La Sonde à Résonance," *L'onde Électrique*, 1965, pp. 1480–1485.

[11]Verboncoeur, J. P., Alves, M. V., Vahedi, V., and Birdsall, C. K., "Simultaneous Potential and Circuit Solution for 1D Bounded Plasma Particle Simulation Codes," *Journal of Computational Physics*, Vol. 104, 1993, pp. 321–328.

[12]Lieberman, Michael A., and Lichtenberg, Allan J., *Principles of Plasma Discharges and Materials Processing*, John Wiley & Sons, 1994.

[13]Haas, James M., Gulczinski III, Frank S., Gallimore, Alec D., Spanjers, Gregory G., and Spores, Ronald A., "Performance Characteristics of a 5 kW Laboratory Hall Thruster," *AIAA Paper AIAA-98-3503*, 1998.

[14]Gilchrist, B. E., Bilén, Sven G., Patrick, Travis A., and Van Noord, Jonathan L., "Bare Electrodynamic Tether Ground Simulations in a Dense, High-Speed Plasma Flow," *AIAA Paper AIAA-2000-3869*, 2000.

[15]Onishi, T., Martinez-Sanchez, M., and Cooke, D. L., "Computation of Current to a Moving Bare Tether," in *Proceedings of the 26th International Electric Propulsion Conference*, paper *IEPC99-217*, 1999.